

Privacy-Preserving Visual Feature Descriptors through Adversarial Affine Subspace Embedding

Mihai Dusmanu¹ Johannes L. Schönberger² Sudepta N. Sinha² Marc Pollefeys^{1,2}

¹ Department of Computer Science, ETH Zürich ² Microsoft

Abstract

Many computer vision systems require users to upload image features to the cloud for processing and storage. Such features can be exploited to recover sensitive information about the scene or subjects, e.g., by reconstructing the appearance of the original image. To address this privacy concern, we propose a new privacy-preserving feature representation. The core idea of our work is to drop constraints from each feature descriptor by embedding it within an affine subspace containing the original feature as well as one or more adversarial feature samples. Feature matching on the privacy-preserving representation is enabled based on the notion of subspace-to-subspace distance. We experimentally demonstrate the effectiveness of our method and its high practical relevance for applications such as crowd-sourced 3D scene reconstruction and face authentication. Compared to the original features, our approach has only marginal impact on performance but makes it significantly more difficult for an adversary to recover private information.

1 Introduction

Visual feature description is a fundamental step in many computer vision tasks such as 3D reconstruction [1, 2] or face recognition [3]. Features can be low-level [1, 4], mid-level [5, 6] or high-level [7, 8], they can be handcrafted or learned, and they are usually represented as vectors in a feature space supporting efficient distance computation for recognition and matching tasks.

Recently, there has been rapid progress in techniques reconstructing the image appearance from the visual features extracted in the original image [9, 10, 11, 12]. This raises privacy concerns since images may contain sensitive information about the scene or subjects.

Increased awareness of privacy concerns have spurred significant efforts to develop privacy-preserving machine learning systems. Researchers have proposed a large body of approaches to tackle the various aspects of the problem, including homomorphic cryptosystems [13], differential privacy [14], federated learning [15], and task-specific solutions [16, 17].

In this paper, we propose a new feature representation suitable for visual recognition and matching tasks that makes it significantly more difficult for an adversary to recover sensitive information. The core idea of our approach is to represent a descriptor point in \mathbb{R}^n as an affine subspace of \mathbb{R}^n passing through the original point. We refer to this process as *lifting*. To confuse an attacker with ambiguous information, we also inject adversarial feature samples as part of the lifted subspaces. Descriptor comparison as the core operation in a recognition system is performed directly on the lifted descriptors using either point-to-subspace or subspace-to-subspace distance.

The paper is organized as follows. First, we formally present the idea of lifting and the technique for matching lifted features. Next, we analyze the performance of these features for two applications, a) image matching for crowd-sourced 3D scene reconstruction and b) face authentication. Finally, we demonstrate that our proposed representation is resilient to potential privacy attacks. The code of our method and the evaluation protocol will be released as open-source.

2 Related Work

We first broadly review the features used for the applications considered in this paper. We then review existing work on privacy attacks on image features and defense mechanisms.

Feature Descriptors. In the traditional local feature extraction paradigm, after keypoint detection and shape estimation, normalized patches are extracted from images. Feature description takes a patch as input and outputs an n -dimensional vector. Handcrafted local descriptors are based on direct pixel sampling [18] or a histogram of image gradients [1, 4]. With the recent advances in deep learning, researchers have developed trainable descriptors using different triplet [19] or list-wise [20] losses and hard-negative mining techniques [21]. Local features have been successfully used for tasks such as large-scale 3D reconstruction from crowd-sourced images [2] and image retrieval [22].

Similarly, face recognition algorithms start by face detection and alignment producing a canonical face image [23]. Early works have shown that a well chosen low-dimensional subspace of pixel-space is enough to obtain a good recognition performance [3]. More recently, convolutional neural networks (CNNs) have become the method of choice for face descriptors. These networks are trained either for classification [24] or for direct embedding using different versions of the triplet loss [25, 26].

Privacy Attacks. Weinzaepfel *et al.* [9] proposed a method for reconstructing images from their local features using a database of patches with associated descriptors. Dosovitsky and Brox [10, 27] extended on this work by using a CNN and perceptual losses, while Pittaluga *et al.* [28] reconstructed images from sparse 3D point clouds. Similarly, Zhmoginov and Sandler [11] and Mai *et al.* [12] proposed methods for recovering face images from their descriptors. Moreover, they showed that the reconstructions can be used by an attacker to fool an authentication system.

Privacy-Preserving Methods. *Differential privacy* [14] expands upon Dalenius [29] by formalizing the problem of querying a database without inadvertently releasing information distinguishing the individual entries. We refer to [30] for an extended overview. Applications such as facial authentication and visual reconstruction are specific to each individual so it is not obvious how to use differential privacy in these cases.

McMahan *et al.* [31] introduced *federated learning*, a distributed client-server framework for training a model, where training data remains with the clients, thus offering better privacy guarantees. Kairouz *et al.* [15] reviews the topic and discusses open problems. However, we address a different setting, where tasks require image features computed by clients to be shared with the server. In this context, our approach makes it difficult to recover private image information from the shared features.

Existing works on local features extract features in the cloud from encrypted images using different homomorphic cryptosystems [32, 33]. In practice, these approaches are usually computationally expensive. Jiang *et al.* [34] proposed an alternative by additively splitting the image into two ciphertext matrices using a private prime modulus. These methods guarantee that the original images remain private, but they do not prevent information leakage by inverting the obtained local features.

Speciale *et al.* [16, 17] proposed solutions tailored to image-based localization where geometric information is concealed by lifting 2D or 3D points to randomly oriented lines passing through the original locations. Subsequently, they used specialized solvers [35, 36] to compute camera pose. We draw inspiration from their work, but instead lift descriptors to higher dimensional affine subspaces.

3 Method

The entire analysis will be done in \mathbb{R}^n , where n is the dimensionality of the original descriptors. We denote $\text{span}(v_1, \dots, v_m) = \{\sum_{i=1}^m \lambda_i v_i | \lambda_i \in \mathbb{R}\}$ the linear span of a set of vectors $v_i \in \mathbb{R}^n$. An m -dimensional affine subspace \mathcal{A} can be represented as the sum of a translation vector a_0 and a linear subspace $\text{span}(a_1, \dots, a_m)$, giving $\mathcal{A} = a_0 + \text{span}(a_1, \dots, a_m)$. The core idea of our method is to lift the original descriptor $d \in \mathbb{R}^n$ to an m -dimensional affine subspace $\mathcal{D} \subset \mathbb{R}^n$ satisfying $d \in \mathcal{D}$. There are two major challenges that need to be addressed. Firstly, one needs to define a distance function that can be used to reliably compare descriptors under this representation. Secondly, the affine subspaces should conceal the true descriptor d such that an attacker is unable to recover it.

3.1 Distance Function

An essential task for most downstream applications is descriptor comparison using distance measures. In our analysis, we restrict ourselves to the Euclidean distance (denoted $\|\cdot\|$) as it is the most commonly used. To compute the distance between private features, we either use the orthogonal point-to-subspace or subspace-to-subspace distance, as defined next.

Point-to-Subspace Distance. To compute the distance between a private descriptor d lifted to an affine subspace \mathcal{D} and an original descriptor e , one can use the point-to-subspace distance defined as:

$$\text{dist}(\mathcal{D}, e) = \min_{x \in \mathcal{D}} \|e - x\| = \|e - p_{\perp}^{\mathcal{D}}(e)\| , \quad (1)$$

where $p_{\perp}^{\mathcal{D}}(e)$ denotes the orthogonal projection of e onto the subspace \mathcal{D} . Since $d \in \mathcal{D}$, the inequality $\text{dist}(\mathcal{D}, e) \leq \|e - d\|$ holds.

Subspace-to-Subspace Distance. To compute the distance between two private descriptors d, e represented as affine subspaces \mathcal{D}, \mathcal{E} , one can use the subspace-to-subspace distance defined as:

$$\text{dist}(\mathcal{D}, \mathcal{E}) = \min_{x \in \mathcal{D}, y \in \mathcal{E}} \|y - x\| . \quad (2)$$

Similarly to the previous case, since $d \in \mathcal{D}, e \in \mathcal{E}$, the inequality $\text{dist}(\mathcal{D}, \mathcal{E}) \leq \|e - d\|$ holds. We denote $x^* = d_0 + \sum_{i=1}^m \alpha_i d_i \in \mathcal{D}, y^* = e_0 + \sum_{i=1}^m \beta_i e_i \in \mathcal{E}$ a pair of points that realizes the minimum, where m is the subspace dimensionality and $\alpha, \beta \in \mathbb{R}^m$. A sufficient and necessary condition for $\text{dist}(\mathcal{D}, \mathcal{E}) = \|y^* - x^*\|$ is that the line $y^* - x^*$ is orthogonal to both \mathcal{D} and \mathcal{E} :

$$\begin{cases} (y^* - x^*)^T d_i = 0 \\ (y^* - x^*)^T e_i = 0 \end{cases} \Leftrightarrow \begin{cases} (e_0 - d_0)^T d_i = \sum_{j=1}^m \alpha_j d_i^T d_j + \sum_{j=1}^m \beta_j (-d_i^T e_j) \\ (e_0 - d_0)^T e_i = \sum_{j=1}^m \alpha_j e_i^T d_j + \sum_{j=1}^m \beta_j (-e_i^T e_j) \end{cases} . \quad (3)$$

This system can be represented under the following compact form:

$$\begin{bmatrix} DD^T & -DE^T \\ ED^T & -EE^T \end{bmatrix} \begin{bmatrix} \alpha \\ \beta \end{bmatrix} = \begin{bmatrix} D \\ E \end{bmatrix} (e_0 - d_0) , \quad (4)$$

where $D = [d_1 \dots d_m]^T, E = [e_1 \dots e_m]^T \in M_{m \times n}(\mathbb{R})$.

Supposing that the basis of each subspace is orthonormal ($DD^T = EE^T = I$), the system becomes:

$$\begin{bmatrix} I & -DE^T \\ ED^T & -I \end{bmatrix} \begin{bmatrix} \alpha \\ \beta \end{bmatrix} = \begin{bmatrix} D \\ E \end{bmatrix} (e_0 - d_0) . \quad (5)$$

Thus, finding the subspace-to-subspace distance requires solving a linear system with $2m$ unknowns and equations. Let $M = -DE^T$. Under the assumption that $I - MM^T$ is invertible, the block-matrix inversion formula can be used to rewrite Eq. 5 as follows:

$$\begin{bmatrix} \alpha \\ \beta \end{bmatrix} = \begin{bmatrix} (I - MM^T)^{-1} & (I - MM^T)^{-1} M \\ -M^T (I - MM^T)^{-1} & -M^T (I - MM^T)^{-1} M - I \end{bmatrix} \begin{bmatrix} D \\ E \end{bmatrix} (e_0 - d_0) . \quad (6)$$

Note that depending on the subspace dimensionality m , it can be more efficient to formulate the problem using the dual representation of the subspace as the intersection of $n - m$ hyperplanes. We provide a derivation and further discussion for the dual setting in the supplementary material.

3.2 Affine Subspace Embedding

Each subspace embedding is defined by a translation vector d_0 and a basis $\{d_1, \dots, d_m\}$. The choice of these and the distribution of the original descriptors has significant impact on the effectiveness of our approach and the required dimensionality m of the subspace to achieve sufficient privacy preservation. For example, it is common practice to ℓ_2 -normalize descriptors [1, 21, 25, 26]. In this case, lifting descriptors to affine lines ($m = 1$) is thus not secure, because lines only intersect the unit hyper-sphere in at most 2 points, while one of those is typically not plausible. Any value of $m > 1$ generally produces an infinity of intersection points. In the following, we detail different lifting strategies that will be evaluated in the experimental section.

Translation Vector. The origin can be set to any point in the subspace, except the vector d itself as it is precisely what we must conceal. Thus, we randomly select a point in the subspace, as follows:

$$d_0 = d + \sum_{i=1}^m \alpha_i d_i \text{ where } \alpha_i \sim \mathcal{U}([-1, 1]) . \quad (7)$$

Random Basis. One could sample random direction vectors for the linear subspace, *i.e.*, $d_i \sim \mathcal{U}([-1, 1])^n$ referred to as *random lifting*. As shown in our experiments, we found this approach to be vulnerable to relatively simple privacy attacks.

Adversarial Basis. To increase the security of the lifted features, one can ensure that the subspace passes through different regions of the descriptor manifold. An efficient implementation could use a database of real-world descriptors $W = \{w_1, \dots, w_s\}$ as an approximation of the manifold and sample the basis vectors as $d_i = w_i - d$, where $w_i \sim \mathcal{U}(W)$. We call this approach *adversarial lifting*, as it intentionally introduces plausible ambiguity in the subspace to conceal the true information. A defender can intentionally choose adversarial samples to hide specific private information, *e.g.*, to hide the gender of a person, one can pick a sample from another gender, as shown in our experimental evaluation. As adversarial sampling adds additional security, it also reduces descriptor matching accuracy, because the chance of accidental subspace collisions increases. To balance the accuracy and security trade-offs, one can also merge the adversarial and the random lifting into a *hybrid lifting*, where a subset of the basis vectors are random and the rest is composed of adversarial samples.

4 Experimental Evaluation

In this section, we evaluate our method on two highly relevant practical applications. First, we experiment with local features on the task of image matching for 3D reconstruction. Second, we apply our method on global image features for face verification. We evaluate these two settings in terms of the level of privacy preservation as well as the induced accuracy and completeness trade-offs. As we cannot give any theoretical guarantees on privacy preservation, we challenge our method with potential privacy attacks and thereby empirically demonstrate the effectiveness of our approach.

4.1 Local Image Features

In order to demonstrate the robustness and generalizability of our approach, we perform our experiments using the arguably most popular hand-crafted local feature (SIFT [1]) as well as a recent state-of-the-art learned descriptor (HardNet [21]). Both descriptors are by default ℓ_2 -normalized.

4.1.1 Subspace Selection

To build the database for adversarial lifting, we cluster 10 million features extracted in 60,000 images from the Places365 dataset [37] into $s = 256,000$ clusters using spherical k-means [38]. In the context of 3D computer vision tasks, it is usually desirable to have many thousands of features per image [39]. Let us consider the case of lifting to descriptor planes ($m = 2$) using uniform random sampling from the database of 256,000 centroids. Given an image pair with 8,000 descriptors per image, for each feature in the second image, there is a $1/16$ chance of sampling a feature already selected in the first one. Such a collision causes subspace intersections and thus leads to wrong feature matches. The effect of wrong matches is further exacerbated due to typical matching filtering strategies such as mutual nearest neighbor check or ratio-test [1].

To reduce the number of wrong matches, we randomly split the database into $S = 16$ pairwise disjoint sub-databases W_1, \dots, W_S satisfying $W = \cup_{i=1}^S W_i$, $\text{card}(W_i) = s/S$. For an image I , we then first randomly select a sub-database $\mathcal{W} \sim \mathcal{U}(\{W_1, \dots, W_S\})$. Next, the basis vectors are generated using only elements of \mathcal{W} , *i.e.*, $v_i = w_i - d$, where $w_i \sim \mathcal{U}(\mathcal{W})$. If two images select different sub-databases in this *sub-adversarial lifting* strategy, the probability of random collision is 0. For images using the same sub-database, the number of collisions is very high. Overall, with this strategy, instead of degrading the matching performance for all image pairs, we achieve good matching performance in $15/16$ cases. In addition, we also evaluate a *sub-hybrid lifting* strategy, where half of the basis vectors are random and the other half uses a sub-database.

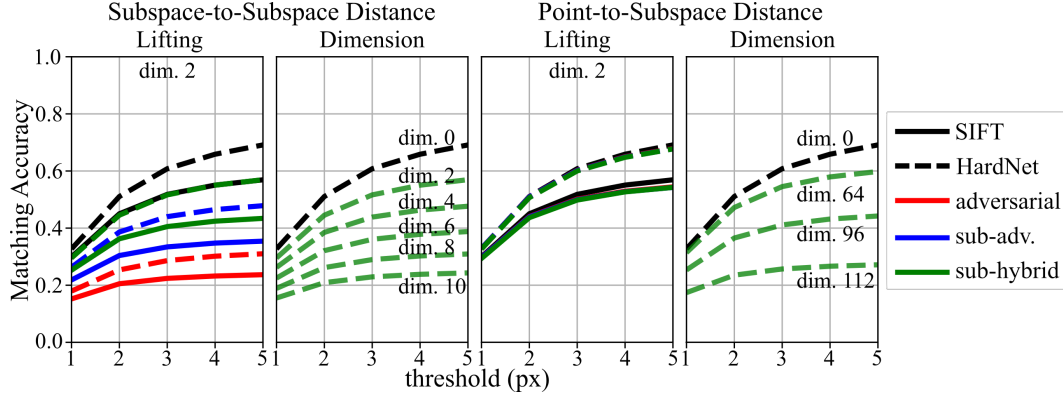


Figure 1: **Matching evaluation.** We plot the mean matching accuracy at different thresholds on the HPatches sequences [40] with different lifting methods and dimensions. HardNet outperforms SIFT on this benchmark and this ordering is respected after lifting as well.

4.1.2 Image Matching

We start by comparing raw descriptors with their private counterparts on the image sequences from the HPatches dataset [40]. This dataset consists of 116 scenes with 6 images each: 57 of them exhibit illumination changes, while the other 59 show significant viewpoint changes. For each scene, we match the first image against the other 5 yielding 580 image pairs in total. The standard protocol introduced in [41] reports the mean matching accuracy of a mutual nearest neighbors matcher for different values of the threshold up to which a match is considered correct.

Figure 1 shows the results for both SIFT and HardNet with different distances, lifting methods, and lifting dimensions. We do not show results with random lifting, since they perform identically with their original counterparts. As mentioned above, the adversarial lifting performs very poorly for local features due to subspace collisions. This is, in part, addressed by the use of sub-databases. Finally, sub-hybrid lifting further improves the results. The point-to-subspace distance only preserves the privacy of one image and is useful for cloud- and client-based visual localization systems, equivalent to Speciale *et al.* [16, 17]. This asymmetric distance is able to achieve good matching performance even for very high lifting dimensions.

4.1.3 Structure-from-Motion


Next, we integrate the best performing private representation from above (sub-hybrid lifting) into an end-to-end 3D reconstruction pipeline [42] and evaluate it on the crowd-sourced 3D reconstruction benchmark from [39]. We first retrieve the top 50 most similar images for each image using NetVLAD [43] and only match against those. Next, we run geometric verification (with a minimum inlier ratio of 0.1) followed by sparse reconstruction using COLMAP [42] and finally report the reconstruction statistics in Table 1. For this evaluation, we preserve the privacy of all input images.

As already observed in our image matching evaluation, the private features come with accuracy trade-offs and we observe a similar pattern here. As we increase the dimensionality of the subspace, the reconstruction completeness degrades accordingly. Despite the fewer number of registered images, the 3D models remain relatively accurate and clearly distinguishable. The generally lower track length for private features is caused by missing matches leading to longer feature tracks being split into multiple smaller ones.

4.1.4 Privacy Attack

For analyzing attacks on our method, we provide the adversary with multiple tools. We assume that they gained access to our lifting database. They also have access to an oracle that, given a list of possible attack descriptors for a private descriptor, returns the closest one to the original descriptor. Finally, they have a CNN that reconstructs images from local features. We trained two such networks on the MegaDepth [44] dataset for inverting Difference-of-Gaussians (DoG) keypoints with SIFT and HardNet descriptors respectively using the architecture and loss from [10].

Table 1: **Local Feature Evaluation Benchmark.** We report different reconstruction statistics on large internet photos of landmarks [39]. The private version of HardNet (sub-hybrid lifting to dim. 2) performs on par with raw SIFT.

Dataset	Method	Reg. images	Sparse points	Track length	Reproj. error	
<i>Madrid Metropolis</i> 1344 images	SIFT	400	28,862	7.01	0.72	
	SIFT - dim. 2	302	17,232	6.37	0.59	
	SIFT - dim. 4	227	11,461	5.54	0.56	
	HardNet	449	33,233	7.13	0.95	
	HardNet - dim. 2	369	25,162	7.13	0.76	
	HardNet - dim. 4	272	14,790	6.90	0.62	
<i>Gendarmenmarkt</i> 1463 images	SIFT	896	74,348	6.37	0.84	
	SIFT - dim. 2	783	64,554	5.44	0.71	
	SIFT - dim. 4	458	33,291	5.23	0.60	
	HardNet	1020	95,894	6.54	0.95	
	HardNet - dim. 2	891	86,591	6.13	0.83	
	HardNet - dim. 4	772	62,025	5.79	0.73	
<i>Tower of London</i> 1576 images	SIFT	635	33,233	7.13	0.95	
	SIFT - dim. 2	525	55,439	6.58	0.61	
	SIFT - dim. 4	439	37,819	6.10	0.56	
	HardNet	743	70,437	7.65	0.86	
	HardNet - dim. 2	601	65,773	7.39	0.71	
	HardNet - dim. 4	503	48,574	6.93	0.64	

We propose the following attack methodology: for each private representation \mathcal{D} associated to a descriptor d , the database is used to retrieve the K closest elements to the subspace a_1, \dots, a_K . Next, these attack descriptors are provided to the oracle, which returns the closest one to the original descriptor d , i.e., $j = \arg \min_{i \in \{1, \dots, K\}} \|a_i - d\|$. The descriptor a_j is then used as an approximation to the original descriptor. We also consider a version where the reconstructed descriptor is obtained by orthogonal projection of a_j to the subspace \mathcal{D} (denoted by $proj.$). Given the approximated descriptors, the CNN can now be used to reconstruct the original image.

Figure 2 shows some quantitative and qualitative results of the attack on 10 images¹ totaling around 40,000 features with HardNet descriptors. Please refer to the supplementary material for the results with SIFT descriptors and more examples. On the left side, we plot the average distance between the original and the reconstructed descriptor as a function of the number of neighbors K . For this experiment, we used sub-hybrid lifting to planes ($m = 2$). The projected version is always closer, but it is not necessarily on the unit sphere. The dotted lines represent the asymptotic values of each respective curve, i.e., the value for $K = 256,000$. On the right side, we show some visual examples: first the initial image and its counterpart reconstructed from the original descriptors; next we show reconstructions for different lifting methods and values of K . Using the raw descriptors, one can reconstruct, with very high fidelity, the original image (note the readability of the text in the background of the first image). Using random lifting, the attack is also successful on private features. For the sub-hybrid lifting, we can see that, even for large numbers of neighbors and access to an imaginary oracle, the reconstructed image remains far from the original. The general outline of the buildings is reconstructed mainly due to the lack of features in the sky (e.g., third example). However, distinguishing details are not present. In practice, the attacker does not have access to the original descriptor d , so implementing the oracle would be an additional challenge for them.

4.2 Face Descriptors

For this evaluation, we use the best performing ArcFace [26] model as a state-of-the-art deep face descriptor with a ResNet-101 [45] backbone trained on the MS-Celeb-1M dataset [46].

¹We manually selected 2 images from each of the following locations: Hong Kong, London, New York, Paris, and Tokyo. The images were published on flickr.com under a CC BY 4.0 License.

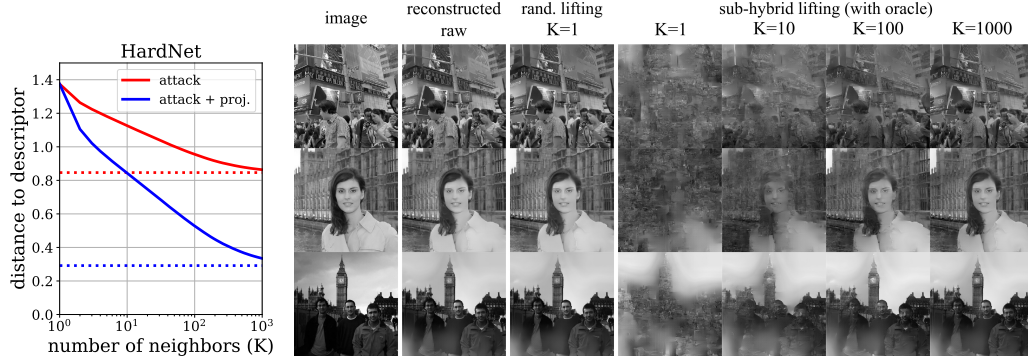


Figure 2: **Image reconstruction.** On the left, we plot the average distance of the reconstructed descriptors to the original one for different values of K , the number of nearest neighbors considered during the attack – features were lifted using sub-hybrid lifting. The dotted lines are the limits of their solid counterparts, *i.e.*, the value when considering all 256,000 database entries. On the right, we show images and their reconstructions: first from the original descriptors, then using the proposed privacy attack with different lifting methods and values of K . Image credit (top to bottom): *pagadooley* (Kevin Dooley), *laylamoran4battersea* (Layla Moran), *martinalvarez* (Martin Alvarez Espinar).

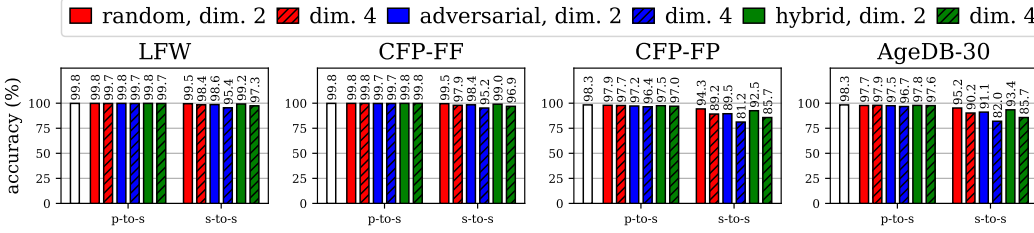


Figure 3: **Face verification.** We show the accuracy on different face verification datasets. The white bar represents the reference accuracy using raw ArcFace descriptors. The point-to-subspace matching (*p-to-s*), where only one descriptor is represented as a subspace, performs within at most 2% of the original descriptors. For the subspace-to-subspace matching (*s-to-s*), the performance drop is more significant in the difficult scenarios (CFP-FP and AgeDB-30), but frontal authentication (LFW and CFP-FF) is still very accurate (95% for the worst performing version – adversarial lifting, dim. 4).

4.2.1 Face Verification

We report face verification accuracy on multiple datasets: LFW [47], CFP [48] (both frontal-frontal denoted FF and frontal-profile denoted FP), and AgeDB-30 [49]. We follow the regular evaluation protocol, notably 10-fold cross validation where, for each fold, the training split is used to determine a distance threshold that separates between same / different identity and the accuracy is computed on the validation split. Finally, the mean classification accuracy over the 10 folds is reported in Figure 3.

We evaluate two scenarios: point-to-subspace (*p-to-s*) matching, where one of the images is represented using the original descriptor and the other one is lifted to a subspace, and subspace-to-subspace (*s-to-s*) matching, where both descriptors are private. As expected, the point-to-subspace matching performs better across the board. The performance on the simple datasets (LFW and CFP-FF) only drops by a few percents in the worst case. For more complex datasets (frontal-profile matching in CFP-FP, large age differences in AgeDB-30), the performance drop is more significant. Nevertheless, the simpler datasets are still very representative of common authentication systems (Microsoft Windows Hello [50], Apple Face ID [51]), making our approach highly relevant for such scenarios.

4.2.2 Privacy Attack

To analyze privacy attacks on ArcFace features, we used FairFace [52], a face dataset with 97,698 images with balanced gender (2 classes) and race (7 classes) annotations. We randomly selected

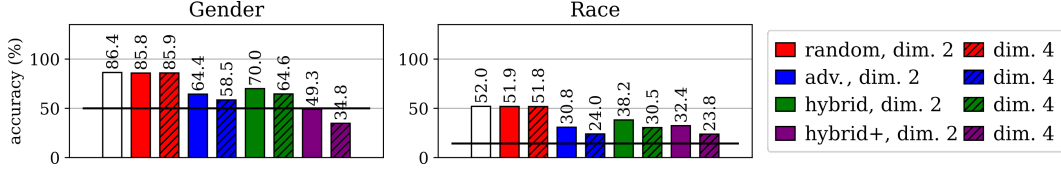


Figure 4: **FairFace**. We report the accuracy of a K-NN classifier trained to predict the gender and race of a subject from their ArcFace descriptor. The black line represents the approximate accuracy of a random classifier. The white bars represent the accuracy on raw ArcFace descriptors. All private representations that use a database for lifting are able to successfully conceal information.

10,000 training images for the database needed by our lifting method. The remaining 76,744 training images were used for the attack. The validation set of 10,954 images is used for evaluation.

We attack an ArcFace feature using a K-nearest neighbors (K-NN) classifier [38] to predict the gender and race of the person. We do this both on the original feature as well as the lifted feature for $K = 10$. We also implemented a variant of our hybrid lifting method (denoted *hybrid+*) that exploits the gender / race of each person. In this variant, each feature is lifted by sampling database entries with a different gender / of a different race, an approach to better conceal these attributes.

The results are reported in Figure 4. The black vertical lines denote the approximate performance of a random classifier. Similar to image matching, pure random lifting is again not very effective at concealing the private attributes. Adversarial lifting has the best results in terms of privacy, but its face verification performance is also the worst. Hybrid lifting offers a trade-off between random lifting (high performance) and adversarial lifting (good for privacy). Finally, the hybrid+ version is most effective at concealing the gender.

5 Limitations and Future Work

In Speciale *et al.* [17], solving the target task (camera pose estimation) reveals the concealed 2D position of some of the image features. Similarly, in our 3D reconstruction task, when two features are successfully matched, the pair of closest points on the two associated affine subspaces provide estimates for the concealed feature descriptors. This implies that the descriptors associated with 3D points triangulated from multiple views are likely to be revealed. Inverting them might allow an adversary to approximately reconstruct the appearance of the stationary part of the scene. However, features extracted from image regions depicting people or other transient objects will generally not be part of the final 3D reconstruction and their appearance is unlikely to be revealed.

For face verification, it is possible to infer the face descriptor after multiple authentications of a person if prior private descriptors are stored. One potential mitigation is to generate near parallel subspaces for a particular subject, although it is unclear how this behaves with respect to the manifold of face descriptors. A potential option would be adding a trusted third-party in the system that receives private descriptors from both client and server and computes the distances without storing any data.

Apart from addressing these limitations, other directions for future work include training descriptors more suitable for lifting and implementing efficient large-scale matching inspired by previous works in the field [53] to enable large-scale applications such as place recognition.

6 Conclusions

We have proposed a novel privacy-preserving feature representation by embedding feature descriptors into affine subspaces containing adversarial samples. To find similar features, nearest neighbor computation is enabled through point-to-subspace and subspace-to-subspace distance. We experimentally demonstrate the high practical relevance of our approach for crowd-sourced 3D reconstruction and face authentication while rendering it difficult to recover sensitive information such as appearance, gender, or race.

Broader Impact

We believe that computer vision can have a positive impact on our daily lives when put to good use through applications such as autonomous driving, robotics, and medical screening. However, we also believe that privacy on the internet should be available to everyone, be it enthusiastic individuals exploring the latest advancements or companies improving their workflow.

Recent works have brought to light privacy vulnerabilities of several state-of-the-art machine learning approaches especially in the case of an untrusted or curious server. Our approach is only a step in the right direction among many others. Nevertheless, we highlighted certain limitations that we expect to be addressed by future works building upon our method.

We hope that our work will motivate the community to continue looking into the privacy issues raised by the use of machine learning in cloud-based applications, be it to challenge existing methods with new attacks or to develop new privacy-preserving methods.

Supplementary Material

This appendix contains the following supplementary information. First, we describe the dual formulation for the point-to-subspace and subspace-to-subspace distance. Next, we discuss the space and time complexity of our matching algorithm. Then, we evaluate the performance of private local features on a long-term visual localization benchmark. Finally, we show more quantitative and qualitative results for the proposed privacy attack on local features in the scenario of an image-based localization service.

A Dual Formulation

Alternative to our formulation in the main paper, an m -dimensional linear subspace of \mathbb{R}^n can also be interpreted as the intersection of $n - m$ hyperplanes. Under this formulation, an affine subspace can be defined by the sum of a translation vector a_0 and the orthogonal subspace of the linear span of a_1, \dots, a_{n-m} , *i.e.*, $\mathcal{A} = a_0 + \text{span}(a_1, \dots, a_{n-m})^\perp$. Throughout the entire section, we suppose that (a_1, \dots, a_{n-m}) is orthonormal, *i.e.*, that $A = [a_1 \dots a_{n-m}]^T$ satisfies $AA^T = I$.

We consider two affine subspaces \mathcal{D}, \mathcal{E} under this representation. Let $(x^*, y^*) \in \mathcal{D} \times \mathcal{E}$ be a solution of the subspace-to-subspace distance, *i.e.*, $\|y^* - x^*\| = \min_{x \in \mathcal{D}, y \in \mathcal{E}} \|y - x\|$. As before, a sufficient and necessary condition for $\text{dist}(\mathcal{D}, \mathcal{E}) = \|y^* - x^*\|$ is that the line $y^* - x^*$ is orthogonal to both \mathcal{D} and \mathcal{E} , *i.e.*, there exist $\mu, \nu \in \mathbb{R}^{n-m}$ such that $y^* - x^* = \sum_{j=1}^{n-m} \mu_j d_j = \sum_{j=1}^{n-m} \nu_j e_j$. Finally, x^*, y^*, μ, ν must satisfy the following constraints:

$$\begin{cases} y^* - x^* = \sum_{j=1}^{n-m} \mu_j d_j = \sum_{j=1}^{n-m} \nu_j e_j \\ d_i^T(x^* - d_0) = 0 \\ e_i^T(y^* - e_0) = 0 \end{cases} \Leftrightarrow \begin{cases} \sum_{j=1}^{n-m} \mu_j d_j - \sum_{j=1}^{n-m} \nu_j e_j = \mathbf{0} \\ d_i^T x^* = d_i^T d_0 \\ e_i^T x^* + \sum_{j=1}^{n-m} \nu_j e_i^T e_j = e_i^T e_0 \end{cases}. \quad (8)$$

This system can be represented under the following compact form:

$$\begin{bmatrix} D & \mathbf{0}_{(n-m) \times (n-m)} & \mathbf{0}_{(n-m) \times (n-m)} \\ E & \mathbf{0}_{(n-m) \times (n-m)} & I \\ \mathbf{0}_{n \times n} & D^T & -E^T \end{bmatrix} \begin{bmatrix} x^* \\ \mu \\ \nu \end{bmatrix} = \begin{bmatrix} D d_0 \\ E e_0 \\ \mathbf{0} \end{bmatrix}, \quad (9)$$

where $D = [d_1 \dots d_{n-m}]^T$, $E = [e_1 \dots e_{n-m}]^T \in M_{(n-m) \times n}(\mathbb{R})$.

In this case, finding the subspace-to-subspace distance can be reduced to solving a linear system with $3n - 2m$ unknowns and equations. This formulation is thus preferable when $m > \frac{3}{4}n$.

For the point-to-subspace distance between a private descriptor under this representation \mathcal{D} and an original descriptor e , the system can be simplified to:

$$\begin{cases} e - x^* = \sum_{j=1}^{n-m} \mu_j d_j \\ d_i^T(x^* - d_0) = 0 \end{cases} \Leftrightarrow \sum_{j=1}^{n-m} \mu_j d_i^T d_j = d_i^T(e - d_0) \Leftrightarrow \mu_i = d_i^T(e - d_0), \quad (10)$$

since $DD^T = I$. Thus, $\text{dist}(\mathcal{D}, e) = \|\sum_{j=1}^{n-m} d_j^T(e - d_0)d_j\| = \|p_{\perp}^{\text{span}(d_1, \dots, d_{n-m})}(e - d_0)\|$.

Table 2: **Aachen Day-Night Localization Challenge.** We report the percentage of localized query images for both day and night scenarios under different camera pose accuracy threshold on the Aachen Day-Night dataset [54].

Method	day queries (824 images)			night queries (98 images)		
	0.25m, 2°	0.5m, 5°	5.0m, 10°	0.5m, 2°	1.0m, 5°	5.0m, 10°
SIFT	84.0%	90.8%	95.0%	29.6%	40.8%	55.1%
SIFT - dim. 16	77.2%	86.7%	90.5%	17.3%	24.5%	33.7%
HardNet	88.3%	94.5%	98.4%	40.8%	59.2%	82.7%
HardNet - dim. 16	85.4%	92.8%	96.0%	29.6%	42.9%	58.2%

B Complexity Analysis

Time Complexity. The complexity of lifting to an m -dimensional subspace is $\mathcal{O}(mn)$ under the supposition that the lifting database offers $\mathcal{O}(1)$ access to a random element (*e.g.*, array, hashtable).

In general, for matching two features lifted to m -dimensional affine subspaces under the primal representation, we require a matrix multiplication $(m \times n)(n \times m)$ (*i.e.*, $M = -DE^T$), the resolution of a system with $2m$ unknowns and equations, and a constant number of additional matrix multiplications between $m \times m$ matrices. Thus, the complexity is $\mathcal{O}(m^2n + m^3)$. Similarly, for the dual representation, the complexity is $\mathcal{O}((3n - 2m)^3)$.

To match two images with N_1 and N_2 local features respectively, we use exhaustive matching which requires computing distances between all pairs of features, *i.e.*, a time complexity of $\mathcal{O}(N_1 N_2 C)$, where C is the complexity of matching two features as defined above.

Runtime. We have implemented CUDA solvers for 2 and 4 dimensional affine subspaces. On the internet datasets, this processes 14 image pairs per second on a single Nvidia RTX 2080Ti.

Space Complexity. For the primal representation, we require one translation vector and m basis vectors totaling $\mathcal{O}((m + 1)n)$ floating point variables instead of $\mathcal{O}(n)$ for the original features. For the dual representation, we require storing $\mathcal{O}((n - m + 1)n)$ floating point variables.

C Aachen Day-Night Localization

We also consider the case of localizing to an already built map on the Aachen Day-Night long-term visual localization dataset [54]. This is equivalent to the scenario tackled by Speciale *et al.* [17], where the goal is to protect the privacy of users of an image-based localization service, such as Google VPS or Microsoft Azure Spatial Anchors. Following the evaluation protocol, we first triangulate the database model based on the given camera poses and intrinsics using DoG keypoints with raw SIFT and HardNet descriptors, respectively. For each query image (824 day-time and 98 night-time), we retrieve the top 50 database images using NetVLAD [43]. We preserve the privacy of all query images with sub-hybrid lifting and use point-to-subspace distance for matching. Finally, we use the COLMAP [42] image registrator to obtain poses that are submitted to the online evaluation system available at <https://www.visuallocalization.net>. Following the standard evaluation protocol, we report the percentage of localized query images for different real-world thresholds in Table 2.

D Privacy Attack

We run the privacy attack described in Section 4.1.4 of the main paper on both SIFT and HardNet private features with sub-hybrid lifting to 2 and 4 dimensional subspaces. SIFT descriptors only take positive values (*i.e.*, in \mathbb{R}_+^{128}), which explains the smaller distance between reconstructed and original when compared to HardNet descriptors taking values in \mathbb{R}^{128} . As expected, a higher lifting dimension increases the distance between reconstructed and original descriptors.

We also show more qualitative results of the attack for SIFT and HardNet in Figures 6 and 7, respectively. All images were published on flickr.com under a CC BY 4.0 License. Image

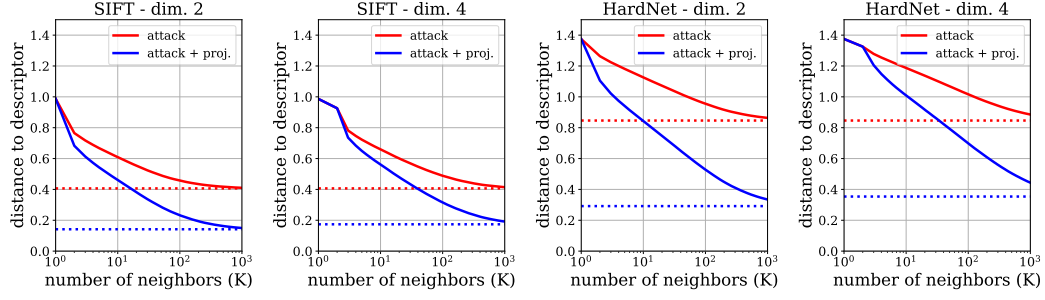


Figure 5: **Image reconstruction – quantitative.** We plot the average distance of the reconstructed descriptors to the original one for different values of K , the number of nearest neighbors considered during the attack – features were lifted using sub-hybrid lifting to dim. 2 and 4. The dotted lines are the limits of their solid counterparts, *i.e.*, the value when considering all 256,000 database entries.

credit (top-to-bottom): twang_dunga (Twang Dunga), scaredykat (krista), bab4lity (wwikgren), herry (Herry Lawford), smemon (Sean MacEntee), laylamoran4battersea (Layla Moran), shankaronline (Shankar S.), martinalvarez (Martin Alvarez Espinar), pagedooley (Kevin Dooley), nukeit1 (James McCauley).



Figure 6: **Image reconstruction – qualitative SIFT.** We show images and their reconstructions: first from the original descriptors, then using the proposed privacy attack with different lifting methods and values of K . For the private versions, descriptors were lifted to planes ($m = 2$).



Figure 7: **Image reconstruction – qualitative HardNet.** We show images and their reconstructions: first from the original descriptors, then using the proposed privacy attack with different lifting methods and values of K . For the private versions, descriptors were lifted to planes ($m = 2$).

References

- [1] David G. Lowe. Distinctive image features from scale-invariant keypoints. *IJCV*, 2004.
- [2] Sameer Agarwal, Yasutaka Furukawa, Noah Snavely, Ian Simon, Brian Curless, Steven M. Seitz, and Richard Szeliski. Building Rome in a Day. *Communications of the ACM*, 2011.
- [3] Matthew Turk and Alex Pentland. Eigenfaces for Recognition. *Journal of Cognitive Neuroscience*, 1991.
- [4] Navneet Dalal and Bill Triggs. Histograms of oriented gradients for human detection. In *Proc. CVPR*, 2005.
- [5] Josef Sivic and Andrew Zisserman. Video Google: A text retrieval approach to object matching in videos. In *Proc. ICCV*, 2003.
- [6] Y-Lan Boureau, Francis Bach, Yann Le Cun, and Jean Ponce. Learning mid-level features for recognition. In *Proc. CVPR*, 2010.
- [7] Ali Sharif Razavian, Hossein Azizpour, Josephine Sullivan, and Stefan Carlsson. CNN Features off-the-shelf: an Astounding Baseline for Recognition. In *Proc. CVPR Workshops*, 2014.
- [8] Matthew D. Zeiler and Rob Fergus. Visualizing and Understanding Convolutional Networks. In *Proc. ECCV*, 2014.
- [9] Philippe Weinzaepfel, Hervé Jégou, and Patrick Pérez. Reconstructing an image from its local descriptors. In *Proc. CVPR*, 2011.
- [10] Alexey Dosovitskiy and Thomas Brox. Inverting visual representations with convolutional networks. In *Proc. CVPR*, 2016.
- [11] Andrey Zhmoginov and Mark Sandler. Inverting face embeddings with convolutional neural networks. *arXiv*, 2016.
- [12] Guancan Mai, Kai Cao, Pong C. Yuen, and Anil K. Jain. On the reconstruction of face images from deep face templates. *IEEE PAMI*, 2018.
- [13] Paillier, Pascal. Public-key Cryptosystems Based on Composite Degree Residuosity Classes. In *Proc. EuroCrypt*, 1999.
- [14] Cynthia Dwork, Frank McSherry, Kobbi Nissim, and Adam Smith. Calibrating noise to sensitivity in private data analysis. In *Proc. TCC*, 2006.
- [15] Peter Kairouz, H. Brendan McMahan, Brendan Avent, Aurélien Bellet, Mehdi Bennis, Arjun Nitin Bhagoji, Keith Bonawitz, Zachary Charles, Graham Cormode, Rachel Cummings, et al. Advances and Open Problems in Federated Learning. *arXiv*, 2019.
- [16] Pablo Speciale, Johannes L. Schonberger, Sing Bing Kang, Sudipta N. Sinha, and Marc Pollefeys. Privacy Preserving Image-Based Localization. In *Proc. CVPR*, 2019.
- [17] Pablo Speciale, Johannes L. Schonberger, Sudipta N. Sinha, and Marc Pollefeys. Privacy Preserving Image Queries for Camera Localization. In *Proc. ICCV*, 2019.
- [18] Michael Calonder, Vincent Lepetit, Mustafa Ozuysal, Tomasz Trzcinski, Christoph Strecha, and Pascal Fua. BRIEF: Computing a local binary descriptor very fast. *IEEE PAMI*, 2011.
- [19] Vassileios Balntas, Edgar Riba, Daniel Ponsa, and Krystian Mikolajczyk. Learning local feature descriptors with triplets and shallow convolutional neural networks. In *Proc. BMVC.*, 2016.
- [20] Kun He, Yan Lu, and Stan Sclaroff. Local Descriptors Optimized for Average Precision. In *Proc. CVPR*, 2018.
- [21] Anastasiya Mishchuk, Dmytro Mishkin, Filip Radenovic, and Jiri Matas. Working hard to know your neighbor’s margins: Local descriptor learning loss. In *Advances in NeurIPS*, 2017.
- [22] Hervé Jégou, Matthijs Douze, Cordelia Schmid, and Patrick Pérez. Aggregating local descriptors into a compact image representation. In *Proc. CVPR*, 2010.
- [23] Kaipeng Zhang, Zhanpeng Zhang, Zhifeng Li, and Yu Qiao. Joint Face Detection and Alignment Using Multi-task Cascaded Convolutional Networks. *IEEE Signal Processing Letters*, 2016.
- [24] Yaniv Taigman, Ming Yang, Marc’Aurelio Ranzato, and Lior Wolf. DeepFace: Closing the gap to human-level performance in face verification. In *Proc. CVPR*, 2014.

- [25] Weiyang Liu, Yandong Wen, Zhiding Yu, Ming Li, Bhiksha Raj, and Le Song. SphereFace: Deep Hypersphere Embedding for Face Recognition. In *Proc. CVPR*, 2017.
- [26] Jiankang Deng, Jia Guo, Xue Niannan, and Stefanos Zafeiriou. ArcFace: Additive Angular Margin Loss for Deep Face Recognition. In *Proc. CVPR*, 2019.
- [27] Alexey Dosovitskiy and Thomas Brox. Generating images with perceptual similarity metrics based on deep networks. In *Advances in NeurIPS*, 2016.
- [28] Francesco Pittaluga, Sanjeev J Koppal, Sing Bing Kang, and Sudipta N Sinha. Revealing Scenes by Inverting Structure From Motion Reconstructions. In *Proc. CVPR*, 2019.
- [29] Tore Dalenius. Towards a methodology for statistical disclosure control. *Statistik Tidskrift*, 1977.
- [30] Cynthia Dwork. Differential Privacy: A Survey of Results. In *Proc. TAMC*, 2008.
- [31] H. Brendan McMahan, Eider Moore, Daniel Ramage, Seth Hampson, and Blaise Agüera y Arcas. Communication-Efficient Learning of Deep Networks from Decentralized Data. *arXiv*, 2016.
- [32] Zhan Qin, Jingbo Yan, Kui Ren, Chang Wen Chen, and Cong Wang. Towards efficient privacy-preserving image feature extraction in cloud computing. In *Proc. ACMM*, 2014.
- [33] Chao-Yung Hsu, Chun-Shien Lu, and Soo-Chang Pei. Image feature extraction in encrypted domain with privacy-preserving SIFT. *IEEE Transactions on Image Processing*, 2012.
- [34] Linzhi Jiang, Chunxiang Xu, Xiaofang Wang, Bo Luo, and Huaqun Wang. Secure outsourcing SIFT: Efficient and privacy-preserving image feature extraction in the encrypted domain. *IEEE Transactions on Dependable and Secure Computing*, 2017.
- [35] Henrik Stewénus, Magnus Oskarsson, Kalle Aström, and David Nistér. Solutions to minimal generalized relative pose problems. In *Proc. CVPR*, 2004.
- [36] Klas Josephson, Martin Byrod, Fredrik Kahl, and Kalle Astrom. Image-based localization using hybrid feature correspondences. In *Proc. CVPR*, 2007.
- [37] Bolei Zhou, Agata Lapedriza, Aditya Khosla, Aude Oliva, and Antonio Torralba. Places: A 10 million image database for scene recognition. *IEEE PAMI*, 2017.
- [38] Christopher M. Bishop. *Pattern Recognition and Machine Learning*. Springer, 2006.
- [39] Johannes L. Schönberger, Hans Hardmeier, Torsten Sattler, and Marc Pollefeys. Comparative evaluation of hand-crafted and learned local features. In *Proc. CVPR*, 2017.
- [40] Vassileios Balntas, Karel Lenc, Andrea Vedaldi, and Krystian Mikolajczyk. HPatches: A benchmark and evaluation of handcrafted and learned local descriptors. In *Proc. CVPR*, 2017.
- [41] Mihai Dusmanu, Ignacio Rocco, Tomas Pajdla, Marc Pollefeys, Josef Sivic, Akihiko Torii, and Torsten Sattler. D2-Net: A Trainable CNN for Joint Detection and Description of Local Features. In *Proc. CVPR*, 2019.
- [42] Johannes Lutz Schönberger and Jan-Michael Frahm. Structure-from-Motion Revisited. In *Proc. CVPR*, 2016.
- [43] Relja Arandjelovic, Petr Gronat, Akihiko Torii, Tomas Pajdla, and Josef Sivic. NetVLAD: CNN architecture for weakly supervised place recognition. In *Proc. CVPR*, 2016.
- [44] Zhengqi Li and Noah Snavely. MegaDepth: Learning single-view depth prediction from internet photos. In *Proc. CVPR*, 2018.
- [45] Kaiming He, Xiangyu Zhang, Shaoqing Ren, and Jian Sun. Deep residual learning for image recognition. In *Proc. CVPR*, 2016.
- [46] Yandong Guo, Lei Zhang, Yuxiao Hu, Xiaodong He, and Jianfeng Gao. MS-Celeb-1M: Challenge of Recognizing One Million Celebrities in the Real World. *Journal of Electronic Imaging*, 2016.
- [47] Gary B. Huang, Marwan Mattar, Tamara Berg, and Eric Learned-Miller. Labeled faces in the wild: A database for studying face recognition in unconstrained environments. Technical report, University of Massachusetts, Amherst, 2007.
- [48] Soumyadip Sengupta, Jun-Cheng Chen, Carlos Castillo, Vishal M. Patel, Rama Chellappa, and David W. Jacobs. Frontal to profile face verification in the wild. In *Proc. WACV*, 2016.

- [49] Stylianos Moschoglou, Athanasios Papaioannou, Christos Sagonas, Jiankang Deng, Irene Kotsia, and Stefanos Zafeiriou. AgeDB: The First Manually Collected, In-The-Wild Age Database. In *Proc. CVPR Workshops*, 2017.
- [50] Microsoft. Windows Hello. <https://blogs.windows.com/windowsexperience/2015/07/25/say-hello-to-windows-hello-on-windows-10/>, 2015.
- [51] Apple. Face ID. <https://support.apple.com/en-us/HT208108>, 2017.
- [52] Kimmo Kärkkäinen and Jungseock Joo. FairFace: Face Attribute Dataset for Balanced Race, Gender, and Age. *arXiv*, 2019.
- [53] Ronen Basri, Tal Hassner, and Lihi Zelnik-Manor. Approximate Nearest Subspace Search with Applications to Pattern Recognition. In *Proc. CVPR*, 2007.
- [54] Torsten Sattler, Will Maddern, Carl Toft, Akihiko Torii, Lars Hammarstrand, Erik Stenborg, Daniel Safari, Masatoshi Okutomi, Marc Pollefeys, Josef Sivic, Fredrik Kahl, and Tomas Pajdla. Benchmarking 6DoF outdoor visual localization in changing conditions. In *Proc. CVPR*, 2018.